Retrieving 65 years of volcano summit deformation from multitemporal structure from motion: The case of Piton de la Fournaise (La Réunion Island)

Allan Derrien, Nicolas Villeneuve, Aline Peltier, François Beauducel

Correspondence to:
N. Villeneuve,
villeneuve@ipgp.fr

Retrieving 65 years of volcano summit deformation from multitemporal structure from motion: The case of Piton de la Fournaise (La Réunion Island)

Allan Derrien[1], Nicolas Villeneuve[1], Aline Peltier[1], and François Beauducel[2]

[1]Observatoire Volcanologique du Piton de la Fournaise, Institut de Physique du Globe de Paris, Sorbonne Paris Cité, Université Paris Diderot, CNRS, La Plaine des Cafres, France, [2]Institut de Physique du Globe de Paris, Sorbonne Paris Cité, Université Paris Diderot, CNRS, Paris, France

Abstract The structure from motion photogrammetry technique enables use of historical airborne photography to achieve high-resolution 3-D terrain models. We apply this method on Piton de la Fournaise volcano (La Réunion), which allows a unique opportunity to retrieve high-resolution (1.5–0.11 m) digital elevation models and precise deformation maps of the volcano since 1950. Our results provide evidence that the summit volume increased throughout the study period, at a stable rate of 2.2 Mm^3/yr between 1950 and 2015, with an acceleration up to 8.0 Mm^3/yr prior to the major 2007 eruption that was accompanied by summit caldera collapse. At the same time, summit deformation was asymmetric, with 9.2 ± 2.5 m of eastward seaward displacement and 1.3 ± 2.5 m to the west during 1950–2015. Our results reveal a temporal evolution in the volcano magma influx rate and deformation. Tracking these fluxes and the long-lived preferential eastern motion is crucial to mitigate risks associated to flank destabilization.

1. Introduction

Characterizing deformation of active volcanoes over long time periods provides essential information for understanding their past and current activity and to forecast their future behavior. It is a crucial issue particularly for active volcanoes that are subject to frequent activity and destabilization (flank deformation and slope instability). Although long-term deformation of a volcano can be revealed from analysis of geological outcrops, as observed for the Campi Flegrei caldera over a 2000 year long period [e.g., *Parascandola*, 1947; *Berrino et al.*, 1984], the first continuous monitoring survey was set up only at the beginning of the last century and only since 1970 in the case of Campi Flegrei [e.g., *Corrado et al.*, 1976, *Berrino et al.*, 1984]. In fact, long time series of deformation data covering more than 50 years has only been achieved at a small number of active volcanoes, these being mainly those monitored by observatories established in the first half of the twentieth century. Even in these cases, the data sets are limited to a small number of spatial points. At the Yellowstone volcanic field (U.S.), based on an initial leveling survey in 1923, the central part of the caldera has risen at a mean rate of 14 ± 1 mm/yr [*Dzurisin et al.*, 2012]. At Kilauea (Hawaii), deformation has been tracked since an initial leveling survey conducted in 1927 [*Jaggar and Finch*, 1929]. Concurrent use of photogrammetry [e.g., *Corre and Giraudin*, 1982; *Zlotnicki et al.*, 1990] and, more recently, availability of satellite-based radar data [e.g., *Massonnet et al.*, 1995; *Rosen et al.*, 1996; *Sigmundsson et al.*, 1999; *Froger et al.*, 2003], allowed the production of spatially continuous high spatial resolution displacement maps. On Piton de la Fournaise, one of the most active basaltic shield volcanoes, located on La Réunion island (France), ground deformation monitoring has been carried out since the establishment of the volcano observatory (OVPF, Observatoire Volcanologique du Piton de la Fournaise) in 1980 using tiltmeters, extensometers, and leveling [e.g., *Bachèlery et al.*, 1982; *Zlotnicki et al.*, 1990; *Peltier et al.*, 2006]. More recently, GNSS (Global Navigation Satellite System) and remote sensing-photogrammetry and Interferometric Synthetic Aperture Radar have enhanced both the temporal and the spatial resolutions of deformation measurements at Piton de la Fournaise [e.g., *Sigmundsson et al.*, 1999; *Froger et al.*, 2003; *Fukushima et al.*, 2005; *Peltier et al.*, 2008, 2015a]. This has enabled characterization and modeling, with more precision, of intereruptive and syneruptive deformation sources. However, regular high spatial resolution spaceborne data for Piton de la Fournaise cover only the last 15 years, giving limited insights into the long-term deformation behavior. Repeated aerial photography surveys conducted over the summit since 1950 enable a precise and exhaustive measurement of Piton de la Fournaise summit déformation, with *De Michele and Briole* [2007] having already

Table 1. Summary of SfM Projects Used in This Study[a]

Date	Photo	Nb of Items	Provider	Resolution		Area (km^2)	GCP	Type	Error (m)	Remarks
				Orthoimage	DEM					
1950	AirPan	3	IGN	1.01	4.08	53	21	Land	7.05	Scars on the photos
1966	AirPan	6	IGN	1.74	3.48	44	15	Land	5.08	
1981	AirPan	49	IGN/OVPF	0.11	0.43	7.17	66	Targets	0.38	Summit only
1997	AirPan	12	OVPF	0.46	1.2	38	27	Targets	1.2	
2003	AirPan	10	IGN	0.62	1.25	53	15	Land	3.46	
2008	AirDigit	50	AIGL	0.13	0.49	5.94	39	Targets	0.52	Summit only
2015	AirDigit	488	OVPF	0.11	0.45	9.18	61	Land	0.24	2010, 2014, and 2015 flows

[a]Photo: AirPan = Airborne Panchromatic images (Scanned for digital processing), AirDigit = Airborne digital images. Nb of items: number of photographs used for SfM reconstruction. Provider: IGN = Institut Géographique National, OVPF = Observatoire Volcanologique du Piton de la Fournaise, and AIGL = Acquisition Information Géo-Localisée. Resolution: resolution (in meters) of the produced Orthoimages and DEMs, respectively. Area: area covered by the model in km^2. GCP: number of used ground control points. Type: GCP type, Land = remarkable landmark measured on site with GNSS receivers (2015) or points assumed to have had no or very small motion and retrieved from georeferenced projects (1950, 1966, and 2003), Targets = stereopreparation GCP, usually 50 × 50 cm white square plexiglas. Error: mean distance (in meter) between assumed position of GCP in the model and measured position.

considered the period 1989 to 1997 using these data. This provides a unique opportunity to achieve a high spatial resolution measurement of the summit deformation over a longer period using structure from motion (SfM) and extends the deformation time series backward by half a century.

Structure from motion photogrammetry is a technique that enables construction of a three-dimensional (3-D) digital model of real objects from photographs [e.g., *Koenderink and Van Doorn*, 1991; *Turner et al.*, 2012]. It is particularly useful for geoscientific observations, because the size of geological objects generally prevents an easy, accurate, and shareable representation using traditional surveying methods but which is the product of SfM. This technique can be used alongside cross correlation, another image analysis technique that computes relative 2-D displacements between sequential images. Both techniques rely on the high-resolution quality of images in order to achieve small-scale measurements (better than 20 cm for our case). Structure from motion and cross-correlation processing of airborne images are robust tools for measuring displacements of geological objects [*De Michele and Briole*, 2007; *Roer et al.*, 2008; *Heid and Kääb*, 2012]. This work aims to (1) use these techniques on a data set of multitemporal airborne images to detect and quantify, for the first time, the evolution of Piton de la Fournaise's summit structure and deformation over the last 65 years and (2) evaluate the potential of these techniques to retrieve past deformation histories for active volcanoes displaying large deformation (metric to decametric). We validate the technique by comparing our most recent results with the deformation database recorded by OVPF.

2. Method

SfM is an automated technique that can create a 3-D model out of digital images of a target object. In particular, SfM uses the differences between images from multiple-viewing points to rebuild the imaged structure in 3-D. First, we applied SfM to process images from seven aerial photography campaigns of the summit area. These were those of the French Institut Géographique National (IGN), the private society "Acquisition Information Géo-Localisée" (AIGL), and OVPF in 1950, 1966, 1981, 1997, 2003, 2008, and 2015 (Table 1). Processing was carried out using Agisoft Photoscan Professional software, which has proven excellent for SfM reconstruction [e.g., *Bolognesi et al.*, 2015]. This allowed us to produce a multitemporal set of orthoimages and digital elevation models (DEMs), georeferenced to UTM coordinates. Each campaign was referenced using the available geodetic ground control data: namely, static natural objects for 1950, 1966, and 2003, and stereo preparation ground control points for 1981, 1997, 2008, and 2015. Next, we cross correlated each consecutive pair of orthoimages using ENVI's "Correlation Image Analysis Software" [*Roer et al.*, 2008; *Heid and Kääb*, 2012]. This allowed us to minimize the decorrelated areas (new lava flows, crater collapses, landslides, etc.) in the output maps. Displacement values in the decorrelated areas were then interpolated from nearby values. The final outputs were multitemporal maps of deformation since 1950, with error estimates for the photogrammetric reconstruction of the model and the coregistration of the image locations for cross correlation. These errors were minimized by constraining the camera parameters in
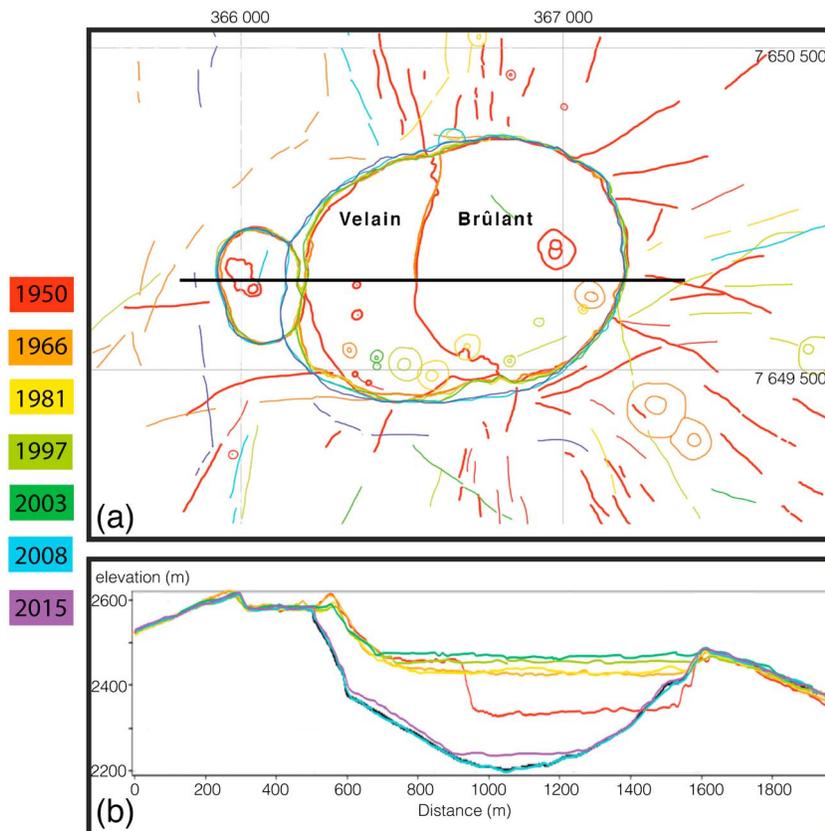
Figure 1. (a) Multitemporal structural map of the summit. Contour of the craters, the eruptive fissures, and vents are shown. Fissures in red predate 1950 and are excluded from our analysis. (b) E-W cross section through Cratère Dolomieu showing changes in elevation with time (see cross-section location in Figure 1a). Coordinates in meters (WGS84, UTM 40S).

Photoscan and running tests using further ground control points than necessary so as to choose those points that yielded the smallest geolocation errors. The details of the reconstruction work, including an estimation of model reliability, are summarized in Table 1. Reliability is assessed according to an error indicator (in meters) that represents the mean distance between the position of a control point, as computed in the model and the assumed value from ground geodesy. The number of control points ensures a globally precise geolocation because positive and negative errors statistically tend to compensate each other.

3. Results

Our processing allowed delivery of new structural (Figure 1) and deformation maps (Figure 2) covering the last 65 years. A precise structural map was created from the set of successive orthoimages, enabling us to accurately locate, in time and space, the consecutive eruptive fissures, and spatter cones active during the study period (Figure 1a). We find that while 30.8% of the eruptive fissures since 1950 are located in the northern half of the summit zone, including Cratère Dolomieu and Cratère Bory, 69.2% are located in the southern half.

The reconstruction of vertical motion allows assessment of the temporal evolution of the crater morphology (filling and collapse cycles, Figure 1b). In 1950, Cratère Dolomieu was composed of two parts: Enclos Velain, to the west, and Cratère Brûlant, to the east. A first collapse of 0.61 Mm^3 inside Enclos Velain was apparent between the 1950 and the 1966 photogrammetric campaigns (Figure 1b) and was dated at 1953 using historical sources [*Bachelery et al.,* 1981; *Michon et al.,* 2013]. Cratère Dolomieu experienced regular infill by lava at a rate of 0.73 ± 0.09 Mm^3/yr between 1950 and 1997 (Figure 3a). The infill rate then increased to 3.30 ± 0.16 Mm^3/yr between 1997 and 2003 (possibly until 2007 and the Cratère Dolomieu collapse). Subsequently, it decreased to 1.00 ± 0.04 Mm^3/yr following the April 2007 collapse. The year 2007 marks a
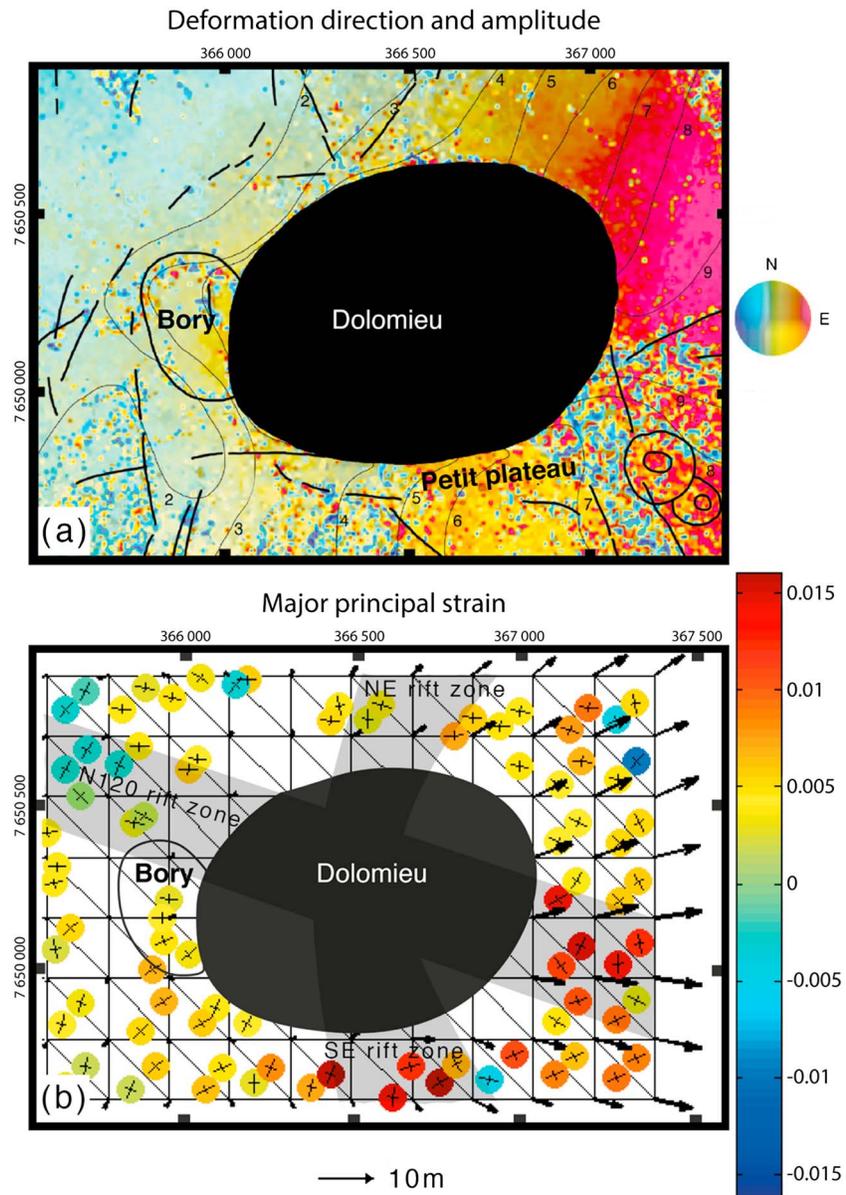
Figure 2. (a) Displacement map of the summit between 1950 and 2015: contours and associated number values give the amplitude, while colors represent the azimuth, as symbolized in the colored circle. The contemporary eruptive vents and fissures are underlined by black lines. (b) Two-dimensional major principal strain map between 1950 and 2015. Colors symbolize the amplitude of strain as given in the color bar and arrows the direction and amplitude of motion. The direction of extension/compression is represented by black cross inside the strain amplitude circles. Coordinates in meters (WGS84, UTM 40S).

particularly important change in the activity at Piton de la Fournaise, probably a consequence of the low-elevation eruption that emitted an unusually high volume of lava (220 Mm^3) [*Roult et al.,* 2012] (Figure 1b). The coincident summit collapse decreased the volume of material inside Cratère Dolomieu by 113.32 ± 2.23 Mm^3, which would compensate 120 years of filling at the 1950–2015 rate. The center of the April 2007 collapse was located 200 m west of the center of the former Cratère Brûlant (Figure 1b).

We were also able to map the planimetric ground displacements between 1950 and 2015 (Figure 2a), as well as the resulting 2-D major principal strain distributions (Figure 2b). The map shows a preferential E-W asymmetrical distribution of ground deformation around the Piton de la Fournaise summit. In contrast, the N-S trend is almost perfectly symmetrical. The amount of motion varies from 1.3 m on the western flank of the summit cone, to 9.2 m on the eastern flank, yielding a maximum time-averaged displacement rate of
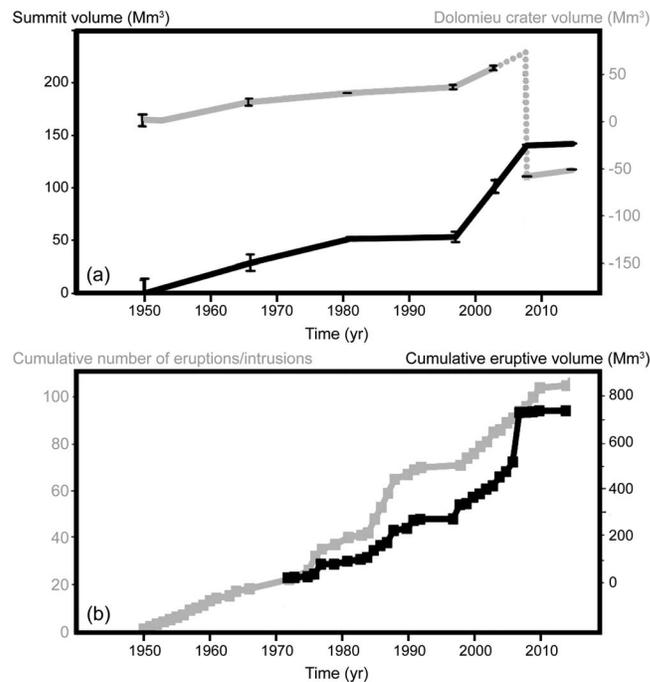
Figure 3. (a) Evolution of the volume inside (grey line) and outside (black line) Cratère Dolomieu in Mm^3 between 1950 and 2015. (b) Cumulative number of dike injections (eruptions/intrusions; in grey) and cumulative erupted volume (in black) as described in *Peltier et al.* [2009], *Roult et al.* [2012], *Michon et al.* [2013], and OVPF recent data.

0.14 m/yr during the 65 yearlong study period (Figure 2a). Some areas near Cratère Dolomieu differ from the general motion trends, especially on the southern flank near the Petit Plateau area (an old pit crater, which is now filled). Here the amplitude of the motion is smaller. In addition, across the eastern half of Cratère Bory the motion is oriented east toward Cratère Dolomieu. It is likely that the collapse of Cratère Dolomieu in 2007, which left a large free space east of Cratère Bory, is the cause of this local motion.

Most of the southeast part of the summit was covered by lava flows overflowing from the crater during the August–December 2006 eruption and presents strong decorrelation due to the change in the topography. However, the signal remains correlated in some areas. The 2-D major principal strain map enables us to identify two zones across which the deformation was greatest (Figure 2b). First, an area located south of Cratère Dolomieu which corresponds to the S-E rift zone.

Here we find a strong E-W extension. Second, an area located N120 from the center of Dolomieu. Here the highest N-S extension values are recorded. The E-W extension is more regularly distributed on the northern flank, along the N-E rift zone. An area in compression is also identifiable northwest of Cratère Bory, indicating that deformation may not propagate farther than the base of the Dolomieu shield on the western flank.

The temporal evolution of the area around the Dolomieu crater was studied using a 1444 × 1908 m window centered on N 366555, E 7650265E (WGS84, UTM 40S coordinates in meters). Outside of Cratère Dolomieu, volume variation is characterized by a mean inflation at a rate of 2.19 ± 0.20 Mm^3/yr (Figure 3a). This trend shows an acceleration after 1997, increasing from 1.66 ± 0.57 Mm^3/yr during 1950–1981, to 8.00 ± 0.48 Mm^3/yr between 1997 and 2008, before dropping to 0.20 ± 0.09 Mm^3/yr after 2008. This latest rate is comparable to that of the 1981–1997 period (0.11 ± 0.24 Mm^3/yr), during which the inflation was slower than the average for the total 1950–1997 period.

The temporal evolution of the planimetric displacements across four areas representative of the four cardinal points around the summit has been plotted and compared with the corresponding GNSS data from the OVPF permanent network, which is available for the period 2008–2015. Comparison of our results with measurements of the permanent GNSS stations SNEG, DERG, DSRG, and BORG (Figure 4a) shows errors on displacement values of 7.8%, 8.4%, 6.5%, and 52%, respectively. At the BORG station, the large error can be explained by its very small displacement. The station is also located very close to the February 2015 vents, leading to a significant overestimation of the motion by cross correlation and thus a high error.

Consistent with the evolution of trends in volumetric changes at the summit, the mean E-W displacement rate accelerates from 22.1 ± 43.7 mm/yr between 1950 and 1997, to 128.9 ± 17.5 mm/yr since 1997 (Figure 4b). The E-W motion then followed a trend similar to that of the 1997–2007 period following the major eruptive and collapse events of 2007. The N-S component of displacement shows the same temporal trends, with a mean rate of 25.0 ± 52.9 mm/yr between 1950 and 1997, increasing to 64.2 ± 24.3 mm/yr between 1997 and 2015, followed by a slight deceleration since 2008 (Figure 4c).
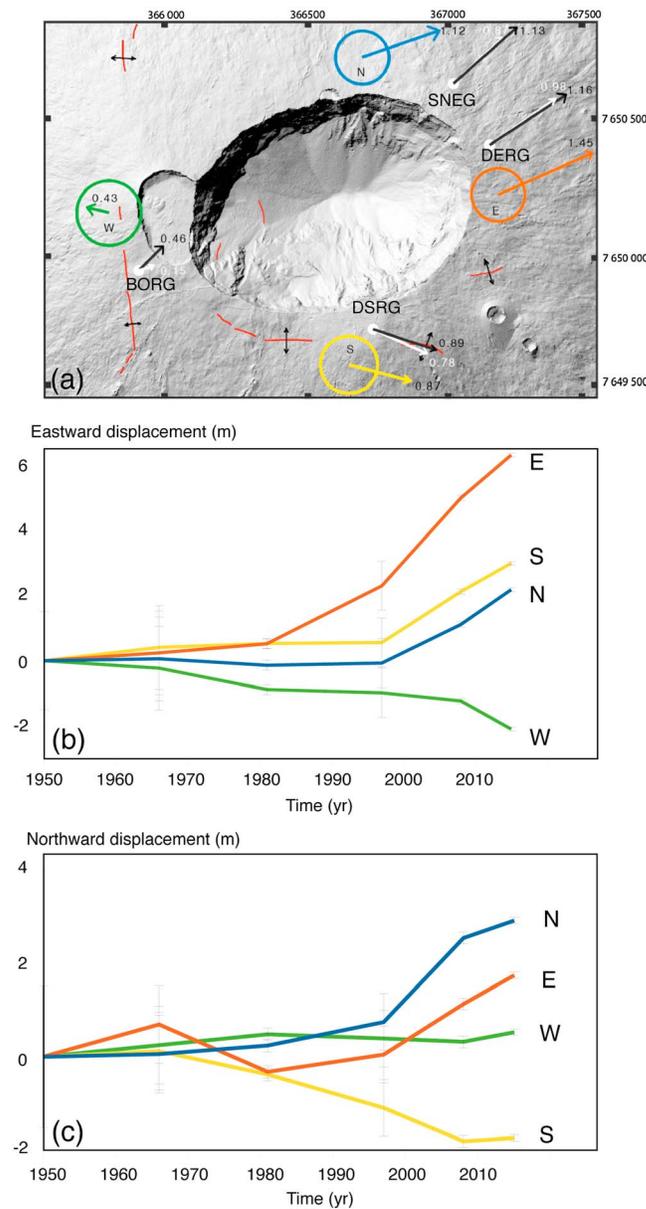
Figure 4. (a) Comparison of the horizontal displacements deduced from airborne photogrammetry (black arrows) and the corresponding permanent OVPF GNSS station (white arrows) between 2008 and 2015. The eruptive fissures that opened during this period are shown by red lines and opening arrows. Coordinates in meters (WGS84, UTM 40S). (b) Eastward and (c) northward cumulative displacement on four representative areas of the north, east, south, and west parts of the summit as identified in (Figure 4a) by the colored circles.

4. Discussion

The high spatial resolution displacement maps computed by our photogrammetric analysis of airborne photographs taken since 1950 has enabled us to characterize, for the first time and with high spatial resolution, the structural evolution and summit deformation of Piton de la Fournaise over more than six decades. Nevertheless, some care needs to be exercised when interpreting the results. The SfM approach results in uncertainties regarding, first, the reconstruction of the structure and, second, the geolocation of the model. Such uncertainties are highest for the models that have no ground control points (i.e., 1950, 1966, and 2003). However, the deformation remains significant even when this uncertainty is considered, and is consistent with the evolution in lava emission volume, which also displays an increase between 1998 and 2007 (Figure 3b).

Combined with the deep seismicity recorded by the OVPF seismic network in 1998 [*Battaglia et al.,* 2005], we have three clues that give evidence of two major changes in the volcano dynamics between 1950 and 2015. Before 1998, the variation in volume both outside and inside of the Dolomieu crater followed a constant trend (Figure 3a), indicating continuity in the volcano output rate for this period. The year 1998 corresponded with refilling of the shallow magma reservoir as seen through seismicity, the refill being continuous until 2007 [e.g., *Peltier et al.,* 2009; *Vlastélic et al.,* 2007]. The shallow reservoir was then emptied during the major April 2007 eruption [e.g., *Staudacher et al.,* 2009; *Roult et al.,* 2012]. This continuous refilling would have been the cause of the high frequency of eruptions recorded between 1998 and 2007, during which a total of 367 Mm^3 of lava was emitted (Figure 3b), an emission rate of about 3.6 times higher than that during 1972–1992 [*Peltier et al.,* 2009]. This would also have been the cause of the acceleration in the deformation (inflation) rate observed at the summit during the same period. Since 2007, and the emptying of the shallow plumbing system, the eruptive regime changed again, being mostly characterized by small summit, or near-summit, eruptions until early 2015 (Figure 3b) [*Peltier et al.,* 2010; *Roult et al.,* 2012]. All of these evidences suggest an increase in the magma influx rate between 1998 and 2007.

Spatially, the E-W asymmetric deformation is consistent with previous studies that have revealed a seaward motion of the eastern flank during recent eruptions [*Froger et al.,* 2003, *Peltier et al.,* 2009; *Rivet et al.,* 2014].

Though the largest displacements occur during eruptions and intrusions, especially for distal eruptions [*Got et al.,* 2013; *Froger et al.,* 2015], intereruptive motion of the lower eastern flank is also present at a lower rate of 10 to 20 mm/yr [*Brenguier et al.,* 2012; *Peltier et al.,* 2015a]. Our results show that this trend has been apparent at least since 1981 (Figure 4b). While the addition of ground control point errors for the 1981 model and the 2015 model accounts for only 6% of the motion, there is a 78% difference between the respective motions of the eastern and the western flanks. The eastern flank presents a small but significant positive northward component that amounts for 25% of its general motion, probably under the influence of the N120 extension zone. Two zones account for most of the E-W and N-S summit extension and correspond to two of the three main rift zones identified on the Piton de la Fournaise edifice, and whose formation is potentially a consequence of the preferential movement of the eastern flank [*Peltier et al.,* 2015b] It is reasonable to infer that the SE and N120 rift zones drive the majority of the preferential motion of the eastern flank over long (decadal-scale) time periods.

5. Conclusions

Our work provides unique insights into changes in the summit structure and deformation of Piton de la Fournaise during the last 65 years. During this time, the summit underwent a continuous increase in its volume at a rate of $2.2 \pm 0.20 \, Mm^3/yr$. This was the result of successive eruptions and intrusions. The deformation was asymmetrically distributed and affected mostly the eastern flank. During this period, while the southeast and N120 rift zones accounted for most of the summit extension, on the northern part of the edifice the strain was more evenly distributed. The deformation rate underwent two major changes, first in 1998 and then in 2007. Both corresponded to major eruptive events that affected the plumbing system and discharge rate, and which marked a change in the eruptive style.

Structure from motion as a tool for retrieving historical topographic data for digital images has given us the opportunity to digitally measure ground deformation with unprecedented accuracy over a 65 year period. Although it is still a very small part in a volcano's life, our results bring new constraints on eruptive dynamics, activity cycles, and implications for volcanic hazard management; extending output and deformation records back by several decades. The evidence of a major long-lived eastward movement of the edifice has to be taken into consideration when it comes to assessing and anticipating the risk of the eastern flank sliding into the sea, on a volcano that has already undergone numerous seaward failures involving large volumes [e.g., *Oehler et al.,* 2008; *Lebas,* 2012].

References

Bachélery, P., et al. (1982), Eruption at Le Piton de la Fournaise volcano on 3 February 1981, *Nature*, *297*, 5865, 395–397.
Bachelery, P., et al. (1981), Eruption at Le Piton de la Fournaise volcano on 3 February 1981, *Nature*, *297*, 395–397, doi:10.1038/297395a0.
Battaglia, J., V. Ferrazzini, T. Staudacher, K. Aki, and J. L. Cheminée (2005), Pre-eruptive migration of earthquakes at the Piton de la Fournaise volcano (Réunion Island), *Geophys. J. Int*, *161*(2), 549–558, doi:10.1111/j.1365-246X.2005.02606.x.
Berrino, G., G. Corrado, G. Luongo, and B. Toro (1984), Ground deformation and gravity changes accompanying the 1982 Pozzuoli uplift, *Bull. Volcanol.*, *47*, 187–200.
Bolognesi, M., A. Furini, V. Russo, A. Pellegrinelli, and P. Russo (2015), Testing the low-cost RPAS potential in 3D cultural heritage reconstruction, *Int. Arch. Photogramm. Remote Sens. Spatial Inf. Sci.*, *XL-5/W4*, 229–235, doi:10.5194/isprsarchives-XL-5-W4-229-2015.
Brenguier, F., et al. (2012), First results from the UnderVolc high-resolution seismic and GPS Network deployed on Piton de la Fournaise Volcano, *Seismol. Res. Lett.*, *83*(1), 97–102, doi:10.1785/gssrl.83.1.97.
Corrado, G., I. Guerra, A. Lo Bascio, G. Luongo, and R. Rampoldi (1976), Inflation and microearthquake activity of Phlegraean fields, Italy, *Bull. Volcanol.*, *40*(3), 169–188.
Corre, P., and P. Giraudin (1982), Une expérience de surveillance photogrammétrique: La route d'accès du tunel routier de Fréjus, *Bulletin d'information de l'IGN*, *45*, 23–31.
de Michele, M., and P. Briole (2007), Deformation between 1989 and 1997 at Piton de la Fournaise volcano retrieved from correlation of panchromatic airborne images, *Geophys. J. Int.*, *169*(1), 357–364, doi:10.1111/j.1365-246X.2006.03307.x.
Dzurisin, D., C. W. Wicks, and M. P. Poland (2012), History of surface displacements at the Yellowstone Caldera, Wyoming, from leveling surveys and InSAR observations: 1923–2008, *U.S. Geol. Surv. Prof. Pap.*, *1788*, 68.
Froger, J.-L., Y. Fukushima, P. Briole, T. Staudacher, T. Souriot, and N. Villeneuve (2004), The deformation field of the August 2003 eruption at Piton de La Fournaise, Reunion Island, mapped by ASAR interferometry, *Geophys. Res. Lett.*, *31*, doi:10.1029/2004GL020479.
Fukushima, Y., V. Cayol, and P. Durand (2005), Finding realistic dike models from interferometric synthetic aperture radar data: The February 2000 eruption at Piton de la Fournaise, *J. Geophys. Res.*, *110*, B03206, doi:10.1029/2t004JB003268.
Got, J.-L., A. Peltier, T. Staudacher, P. Kowalski, and P. Boissier (2013), Edifice strength and magma transfer modulation at Piton de la Fournaise volcano, *J. Geophys. Res. Solid Earth*, *118*, 5040–5057, doi:10.1002/jgrb.50350.
Heid, T., and A. Kääb (2012), Repeat optical satellite images reveal widespread and long term decrease in land-terminating glacier speeds, *Cryosphere*, *6*, 467–478.
Jaggar, T. A., and R. H. Finch (1929), Tilt records for thirteen years at the Hawaiian Volcano Observatory, *Seismol. Soc. Am. Bull.*, *19*(1), 38–51.
Koenderink, J. J., and A. J. Van Doorn (1991), Affine structure from motion, *J. Opt. Soc. Am. A*, *8*(2), 377–385.

Lebas, E. (2012), Processus de démantelement des edifices volcaniques au cours de leur evolution: Application à La Réunion et Montserrat et comparaison avec d'autres edifices, PhD thesis. Université Paris-Diderot, 379 pp.

Michon, L., A. Di Muro, N. Villeneuve, C. Saint-Marc, P. Fadda, and F. Manta (2013), Explosive activity of the summit cone of Piton de la Fournaise volcano (La Réunion island): A historical and geological review, *J. Volcanol. Geotherm. Res.*, *263*, 117–133.

Massonnet, D., P. Briole, and A. Arnaud (1995), Deflation of Mount Etna monitored by spaceborne radar interferometry, *Nature*, *375*, 567–570.

Oehler, J. F., J. F. Lénat, and P. Labazuy (2008), Growth and collapse of the Reunion Island volcanoes, *Bull. Volcanol.*, *70*, 717–742, doi:10.1007/s00445-007-0163-0.

Parascandola, A. (1947), *I Fenomeni Bradisismici det Serapeo di Pozzuoli*, Genovese, Napoli.

Peltier, A., T. Staudacher, P. Catherine, L.-P. Ricard, P. Kowalski, and P. Bachèlery (2006), Subtle precursors of volcanic eruptions at Piton de La Fournaise detected by extensometers, *Geophys. Res. Lett.*, *33*, L06315, doi:10.1029/2005GL025495.

Peltier, A., V. Famin, P. Bachèlery, V. Cayol, Y. Fukushima, and T. Staudacher (2008), Cyclic magma storages and transfers at Piton de La Fournaise volcano (La Réunion hotspot) inferred from deformation and geochemical data, *Earth Planet. Sci. Lett.*, *270*(3–4), 180–188, doi:10.1016/j.epsl.2008.02.042.

Peltier, A., T. Staudacher, P. Bachèlery, and V. Cayol (2009), Formation of the April 2007 caldera collapse at Piton de La Fournaise volcano: Insights from GPS data, *J. Volcanol. Geotherm. Res.*, *184*(1–2), 152–163, doi:10.1016/j.jvolgeores.2008.09.009.

Peltier, A., T. Staudacher, and P. Bachèlery (2010), New behavior of the Piton de La Fournaise volcano feeding system (La Réunion Island) deduced from GPS data: Influence of the 2007 Dolomieu caldera collapse, *J. Volcanol. Geotherm. Res.*, *192*(1–2), 48–56, doi:10.1016/j.jvolgeores.2010.02.007.

Peltier, A., J. L. Got, N. Villeneuve, P. Boissier, T. Staudacher, and V. Ferrazzini (2015a), Long-term mass transfer at Piton de la Fournaise volcano evidenced by strain distribution derived from GNSS network, *J. Geophys. Res. Solid Earth*, *120*, 1874–1889, doi:10.1002/2014JB011738.

Peltier, A., M. Poland, T. Staudacher (2015b), Are Piton de la Fournaise (La Réunion) and Kīlauea (Hawai'i) really "analog volcanoes"? in *Hawaiian Volcanoes: From Source to Surface*, edited by R. Carey, et al., John Wiley, Inc, Hoboken, N. J., doi:10.1002/9781118872079.ch23.

Rivet, D., F. Brenguier, D. Clarke, N. M. Shapiro, and A. Peltier (2014), Long-term dynamics of Piton de la Fournaise volcano from 13 years of seismic velocity change measurements and GPS observations, *J. Geophys. Res. Solid Earth*, *119*, 7654–7666, doi:10.1002/(ISSN)2169-9356.

Roer, I., A. Kaab, and R. Dikau (2008), Rockglacier kinematics derived from small-scale aerial photography and digital airborne pushbroom imagery, *Z. Geomorphol.*, *49*(1), 1–15.

Rosen, P. A., S. Hensley, H. A. Zebker, F. H. Webb, and E. J. Fielding (1996), Surface deformation and coherence measurements of Kilauea volcano, Hawaii, from SIR-C radar interferometry, *J. Geophys. Res.*, *101*(E10), 23,109–23,125, doi:10.1029/96JE01459.

Roult, G., A. Peltier, B. Taisne, T. Staudacher, V. Ferrazzini, A. Di Muro, and The OVPF team (2012), A new comprehensive classification of the Piton de la Fournaise activity spanning the 1985–2010 period. Search and analysis of short-term precursors from a broad-band seismological station, *J. Volcanol. Geotherm. Res.*, *241–242*, 78–104, doi:10.1016/j.jvolgeores.2012.06.012.

Sigmundsson, F., P. Durand, and D. Massonet (1999), Opening of an eruption fissure and seaward displacement at Piton de La Fournaise volcano measured by RADARSAT satellite radar interferometry, *Geophys. Res. Lett.*, *26*, 533–536.

Staudacher, T., V. Ferrazzini, A. Peltier, P. Kowalski, P. Boissier, P. Catherine, F. Lauret, and F. Massin (2009), The April 2007 eruption and Cratère Dolomieu collapse, two major events at Piton de la Fournaise (La Réunion Island, Indian Ocean), *J. Volcanol. Geotherm. Res.*, *184*(1–2), 126–137, doi:10.1016/j.jvolgeores.2008.11.005.

Turner, D., A. Lucieer, and C. Watson (2012), An automated technique for generating georectified mosaics from ultra-high-resolution unmanned aerial vehicle (UAV) imagery, based on structure from motion (SfM) point clouds, *Remote Sensing*, *4*(5), 1392–1410.

Vlastélic, I., A. Peltier, and T. Staudacher (2007), Short-term (1998–2006) fluctuations of Pb isotopes at Piton de la Fournaise volcano (Reunion Island): Origins and constraints on the size and shape of the magma reservoir, *Chem. Geol.*, *244*(1–2), 202–220, doi:10.1016/j.chemgeo.2007.06.015.

Zlotnicki, J., J. C. Ruegg, P. Bachèlery, and P. A. Blum (1990), Eruptive mechanism on Piton de la Fournaise volcano associated with the December 4, 1983, and January 18, 1984 eruptions from ground deformation monitoring and photogrammetric surveys, *J. Volcanol. Geotherm. Res.*, *40*(3), 197–217, doi:10.1016/0377-0273(90)90121-U.